International Journal of Refrigeration 175 (2025) 412–423

Contents lists available at ScienceDirect

International Journal of Refrigeration

journal homepage: www.elsevier.com/locate/ijrefrig

INSTITUT INTERNATIONAL DU FROID
INTERNATIONAL INSTITUTE OF REFRIGERATION

Combining molecular modelling approaches for a holistic thermophysical characterisation of fluorinated refrigerant blends

Daniel Jovell [a], Gerard Alonso [b], Pablo Gamallo [c], Rafael Gonzalez-Olmos [a], Héctor Quinteros-Lama [d,*], Fèlix Llovell [e,*]

[a] Department of Chemical Engineering and Material Science, IQS School of Engineering, Universitat Ramon Llull, Via Augusta 390, 08017, Barcelona, Spain
[b] Departamento de Ingeniería Química, Faculty of Engineering, Universidad de Concepción, Edmundo Larenas 219, Concepción, Chile
[c] Departament de Ciència de Materials i Química Física & Institut de Química Teòrica i Computacional (IQTCUB), Universitat de Barcelona, C. Martí i Franquès 1, 08028, Barcelona, Spain
[d] Departamento de Tecnologías Industriales, Faculty of Engineering, Universidad de Talca., Merced 437, Curicó, Chile
[e] Department of Chemical Engineering, ETSEQ, Universitat Rovira i Virgili, Avda Països Catalans 26, 43007 Tarragona, Spain

ARTICLE INFO

Keywords:
Fluorinated refrigerants
Molecular dynamics
Soft-SAFT EOS
Phase equilibria
Surface tension
Viscosity

ABSTRACT

After Montreal Protocol, hydrofluorocarbons (HFCs) appeared to be a permanent solution for replacing previous ozone-depleting substances. However, their utilisation has now progressively decreased following the Kigali Amendment application in 2016 due to their high global warming potential (GWP). Unsaturated HFCs, such as hydrofluoroolefins (HFOs), are considered feasible alternatives due to their high reaction rates and low atmospheric lifetimes, resulting in very low GWP. However, available data on their physicochemical behaviour still needs to be improved, even with the recent increase in the amount of new experimental data for these systems. In this direction, computational tools provide a quick pathway to screen their properties and complete the information obtained from experimental work. In this contribution, two different molecular modelling tools, molecular dynamics (MD) simulations and the soft-SAFT equation of state (EOS), are combined to compute the coexistence densities, vapour pressure, heat capacity, interfacial tension, and dynamic viscosity of several refrigerant blends based on 3rd and 4th generation compounds, in order to provide a thermodynamic analysis of the properties of these mixtures, addressing them for drop-in replacement purposes. Results from MD are compared with REFPROP data and those from soft-SAFT, where the capacities of both modelling methods are addressed. In general, quantitative agreement is achieved using the two approaches, offering a framework to screen these properties for new mixtures.

1. Introduction

In 2022, the IPCC's Climate Change: Impacts, Adaptation, and Vulnerability report (IPCC, 2022) emphasised the interconnection of climate, biodiversity, and socioeconomic and state models. The report showed that *half-measures to address climate risks are no longer an option*. In the same direction, two hundred seventy authors and many collaborators concurred that a lack of global urgency results in insufficient political leadership and commitment from the business and public sectors. The findings from the 34 000 reference materials indicate that immediate actions are required to avoid a temperature increase higher than 1.5 °C, a plausible scenario given the current tendency. As a result, the delay in taking effective action accelerates the closing of the remaining window of opportunity.

In addition to the reported financial, governmental, institutional, and political barriers to adaptation, the international scientific community has been committed to mitigating the influence of the Greenhouse Gases (GHG) on global warming. Apart from CO_2, which still accounts for 80% of all GHG emissions (United States Environmental Protection Agency, 2020), fluorinated (F)-gases (including hydrofluorocarbons, perfluorocarbons, sulphur hexafluoride, or nitrogen trifluoride) are also a matter of concern because they exhibit very high Global Warming Potentials (GWPs).

In particular, hydrofluorocarbons (HFCs) are substitutes for stratospheric ozone-depleting substances, e.g., chlorofluorocarbons, hydrochlorofluorocarbons, and halons (Burkholder et al., 2015). Those compounds were developed as an alternative to compounds phased out under the Montreal Protocol application (United Nations Environment Programme Ozone Secretariat, 2020). Nevertheless, administrations

* Corresponding authors.
E-mail addresses: hquinteros@me.com (H. Quinteros-Lama), felix.llovell@urv.cat (F. Llovell).

https://doi.org/10.1016/j.ijrefrig.2025.03.026
Received 17 October 2024; Received in revised form 20 February 2025; Accepted 19 March 2025
Available online 28 March 2025

are taking regulatory action to control these F-gases as part of their policy to combat climate change. In October 2016, the Kigali Amendment (Amendment to the Montreal Protocol, 2016) added HFCs to the list of controlled substances under the Montreal Protocol. The European Union (EU) also adopted two legislative acts in this regard. From one side, the very recent 2024/573 Regulation, which repeals previous F-gas 517/2014 Regulation (Regulation (EU), 2024) and strengthens controls on F-gases by adding 23 new substances, phasing out products with high GWP by specific dates, and creating a F-gas portal for quota management and reporting of all F-gases and equipment. From the other side, the MAC Directive (Directive 2006/40/EC), which prohibits the use of F-gases with a GWP of more than 150 times greater than CO_2 in new types of cars and vans introduced from 2011 or produced from 2017. These otherwise necessary restrictions severely impact the entire refrigeration and air conditioning sector, where high GWP HFCs are still widely established in commercial equipment. Indeed, most commercial refrigeration systems installed or used today in Europe are based on HFCs. The most used synthetic refrigerants are R134a (1,1,1,2-tetrafluoroethane), R404A (a ternary blend comprised of R134a, R125, and R143a), R407F (comprised of R125, R134a and R32) and R410A (a blend between R125 and R32) (Zeiger et al., 2016).

In the last decade, unsaturated fluorinated compounds like hydrofluoroolefins (HFO) have emerged as alternative refrigerants, since they exhibit low GWP and nearly null ozone depletion potential (ODP). However, despite having suitable thermophysical properties, most of these refrigerants are flammable (classified as A2L according to the ASHRAE classification), meaning their use as single compounds may be limited. Additional drawbacks of using pure HFOs as alternative refrigerants are their relatively lower volumetric cooling capacity (VCC) (compared to HFC blends'), as well as their degradation into polyfluoroalkyl substances (PFAS), particularly in trifluoroacetic acid (TFA) (Arp et al., 2024), due to their short atmospheric lifetime, as a consequence of fugitive emissions. Therefore, current developments promote the combination of HFCs and HFOs to balance technical, safety and environmental properties.

The characterisation and development of novel HFOs and their blends have garnered increasing interest from the industry. Meanwhile, the scientific community has sought the ideal combination of thermophysical, environmental, and safety properties. However, the vast range of possible compositions and mixtures necessitates a large number of experimental measurements. To partially address this challenge, molecular-based theoretical approaches, such as molecular simulations and equations of state (EOS), offer valuable insights. These methods can be time- and cost-effective alternatives, while providing reliable results.

Molecular simulations are capable to deliver much detail on the physicochemical behaviour of refrigerants. Among several contributions, it is worth highlighting the work of Raabe and coworkers, who developed transferable force fields to accurately describe the vapour–liquid equilibria, thermophysical properties and transport properties of selected pure HFOs (Raabe and Maginn, 2010a; Raabe, 2016; Petr and Raabe, 2015; Raabe and Maginn, 2010b; Raabe, 2020, 2012) and mixtures with other refrigerants (i.e., HFCs) (Raabe, 2014, 2016, 2017) by molecular simulation. A set of extensively used force fields for HFCs, fitted to reproduce vapour-liquid equilibria, are available regarding fluoromethanes (Fermeglia et al., 2003; Potter et al., 1997) or fluoroethanes (Fermeglia et al., 2003; Peguin et al., 2009; Kelkar et al., 2008), some of which were successfully used in combination of Raabe's force field to model HFC + HFO blends (Raabe, 2016, 2014). In addition to these contributions, the recent works of Befort et al. (2021, 2022) and Wang et al. (2023) provide new sets of parameters for pure HFCs using Machine Learning (ML) techniques, offering a very promising performance. A compilation of past and ongoing molecular simulation studies on 3rd and 4th-generation refrigerants are discussed in Raabe's review (Raabe, 2019).

Equations of state (EOS) have also been addressed to describe the thermophysical behaviour of HFCs and HFOs as an alternative to molecular simulations. Vega and coworkers (Vilaseca et al., 2010; Albà et al., 2023a, 2021) published a consistent thermodynamic model to describe 3rd and 4th generation HFC and HFO-based refrigerants. The soft-SAFT EOS has also proven to be a reliable tool to describe the feasibility of the absorption of different fluorinated refrigerants in ionic liquids (ILs) (Asensio-Delgado et al., 2020), fluorinated ionic liquids (FILs) (Jovell et al., 2020), and newly developed fluorinated deep eutectic solvents (DES) (Demirbek et al., 2024).

However, most of these modelling studies are related to phase equilibria (i.e., saturated density, vapour pressure and solubility in solvents). At the same time, less attention has been paid to other properties of interest. For example, the surface tension is a crucial property required to correlate and predict heat transfer when a phase change occurs, since it influences nucleate boiling and two-phase flow characteristics (Zhelezny et al., 2014), which in turn is critical for identifying new low-GWP alternative refrigerants. However, this is one of the less-studied properties for refrigerants and refrigerant-oil solutions (Zhelezny et al., 2014). Still, it is worth to mention the work of Li et al. (2019), who have calculated the interfacial properties of these systems, including binary HFO/HC blends, using molecular simulations. In a different contribution, a relation between azeotropy and aneotropy in refrigerant blends was found by González-Barramuño and coworkers (González-Barramuño et al., 2022) using SAFT-VR-Mie, demonstrating that interfacial tension could be optimised as well as the temperature glide of the mixture. Another crucial property is the heat capacity, which is essential in the design and optimisation of thermal machines and is usually challenging to obtain theoretically with enough accuracy. The heat capacity is a second-order thermal property and, therefore, is highly sensitive to the thermal fluctuations of the models. A similar scenario is found in mixtures, being the corresponding states principle the most frequently found approach for rendering this property (Gao et al., 2018; Al Ghafri et al., 2019; Sheng et al., 2021). Finally, the evaluation of transport properties of refrigerants and their blends has been scarcely studied. They include the thermal conductivity for determining heat transfer coefficients, and the viscosity for fluid flow behaviour and convection effects, playing an essential role in heat transfer and pressure drop characteristics, which are of paramount importance in the design of refrigerant equipment.

Typically, these properties are currently determined through manufacturers' specific correlations for each fluid (Opteon™ Solutions, 2021) and extended corresponding states (Klein et al., 1997; McLinden et al., 2000) (as implemented in the NIST's Reference Fluid Thermodynamic Transport Property Database (REFPROP) Lemmon et al., 2018). Alternatively, in terms of molecular modelling, the use of SAFT (Llovell et al., 2013) or cubic EOS (Polishuk, 2012) coupled with the free volume theory (FVT) (Allal et al., 2001a,b) or scaling theories (González-Barramuño et al., 2023) are methods that still rely on experimental data, which is scarce for HFO-based blends. However, molecular simulations can provide physical insight into studying the transport and interfacial properties to complement theoretical results without the need for experimental data and are expected to become crucial in analysing such properties shortly.

In this work, a theoretical framework combining molecular dynamics (MD) simulations with the use of the polar soft-SAFT EOS provides a complete thermophysical insight into the description of several alternatives to R410A (50.0 %w of R32 and 50.0 %w of R125) and R407F (30.0 %w of R32, 30.0 %w of R125, and 40.0 %w of R134a), two of the most widely used refrigerants in air conditioning and industrial refrigeration installations (Mota-Babiloni et al., 2017) with very high GWP. The alternative blends include binary refrigerants, such as R454B (31.1 w% of R1234yf and 68.9 w% of R32) and R513A (56.0%w of R1234yf and 44.0 w% of R134a), and the ternary mixture R452B (67.0 %w of R32, 7.0 of R125 %w, and 26.0 %w of R1234yf). Particular emphasis is given to describing surface tension, heat capacities, and viscosities. All these properties, along with the vapour–liquid equilibrium envelope and vapour pressure, have been reproduced using MD and have also been calculated with the polar soft-SAFT EOS, being critically compared with the correlated experimental values provided by REFPROP (v.10.0) (Lemmon et al., 2018).

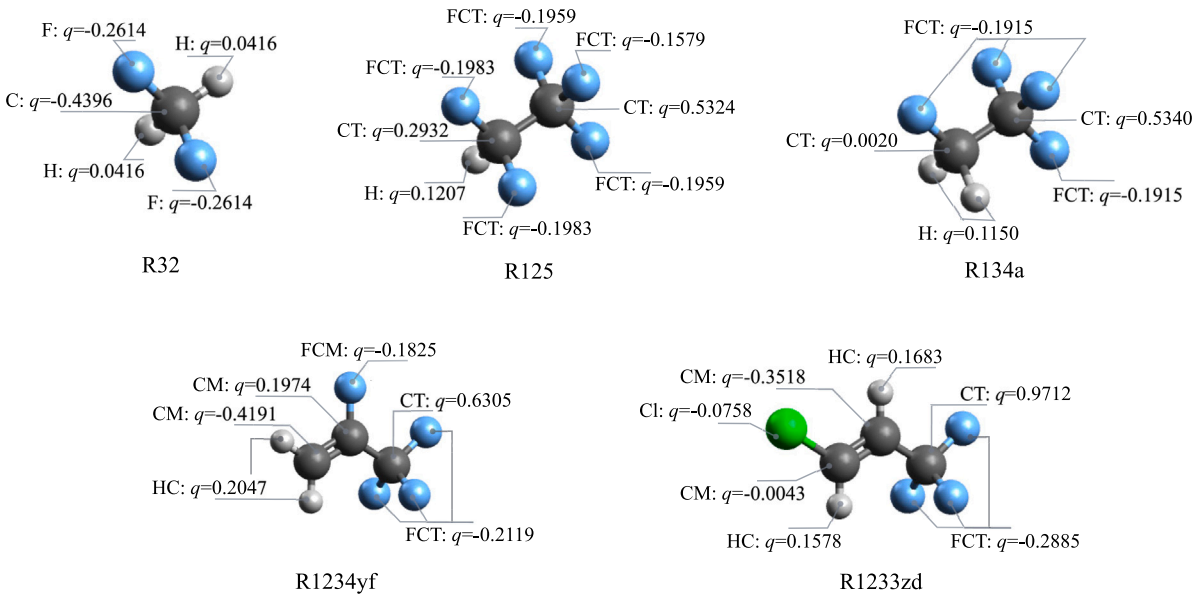

Fig. 1. Structures and partial charges of the refrigerant molecules and nomenclature of the different involved LJ atom types.

2. Background and modelling

2.1. Molecular simulation details

MD simulations for HFCs, HFOs and their mixtures were carried out using the Large-scale Atomic/Molecular Massively Parallel Simulator (LAMMPS) code (Thompson et al., 2022) using the transferable force field of Raabe for R1234yf (Raabe and Maginn, 2010a), R32 (Raabe, 2013), and R1233zd(E) (Raabe, 2015). Parameters for R125 were transferred from equivalent atom types in Raabe and Maginn (2010a) and, following the author's previous works (Raabe, 2013), the parameters for R134a were taken from Peguin et al. (2009). The Lennard-Jones (LJ) bond, angle, and torsional parameters used in the MD simulations are compiled in the Supplementary Material (SM). Molecule-dependent partial charges are shown with their respective atomic labels in Fig. 1.

In this force field, the intermolecular energy of the system was calculated in an atomistic molecular representation *via* a standard LJ (12–6) plus Coulomb pair potentials, as shown in Eq. (1). Originally, homogeneous long-range corrections (hLRC) for LJ were employed to fit the selected force field parameters. However, since interfacial simulations require heterogeneous direct coexistence cells, hLRC cannot be used. For this reason, the missing long-range interactions were accounted by using a large spherical cutoff (22 Å) (Hockney and Eastwood, 1988; Janeček, 2006; Duque and Vega, 2004; Martínez-Ruiz et al., 2015; Müller et al., 2021) and the long-range Coulombic energy was computed with the Particle-Particle/Particle-Mesh (PPPM) method.

Each atom partial charge was obtained from the previously mentioned works, where the authors employed the CHELPG method from *ab-initio* calculations in Gaussian 16 (Frisch et al., 2016). The only exception was R125, whose partial charges were originally not reported and were obtained in this work with an equivalent methodology at the HF/6-31G* level of theory. It is important to note that quantum effects can have a severe impact in reproducing thermophysical properties of low molar mass fluids at low temperature (Aasen et al., 2019). In particular, liquid densities, viscosities and heat capacities at low temperatures tend to be overestimated while vapour pressure are typically underestimated in classical fluid representations, which quantum corrections tend to address. Even though temperatures explored in this contribution range from room temperature down to 180 K, quantum effects are not considered for two reasons: (i) the modelled refrigerants are relatively heavy (from 52.0 g/mol to 130.5 g/mol), so corrections are expected to be small (Costa Cabral et al., 2001), and (ii) the force field selected did not consider quantum corrections during its fitting but still provides high accuracy in reproducing the thermophysical properties of HFCs and HFOs, specially at low temperatures. Finally, the intramolecular interactions are treated *via* a harmonic bond stretching, a harmonic angle bending, and a cosine-expansion series torsion term, as in Eq. (2), where *b*, *a*, and *t* refer to *bond*, *angle*, and *torsion*, respectively.

$$E_{ij} = 4\varepsilon_{ij}\left(\left(\frac{\sigma_{ij}}{r_{ij}}\right)^{12} - \left(\frac{\sigma_{ij}}{r_{ij}}\right)^{6}\right) + \frac{1}{4\pi\epsilon_0 r_{ij}} q_i q_j \tag{1}$$

$$\begin{aligned} E_{intra} = &\sum_b K_b \left(r_{ij} - r_{ij,0}\right)^2 + \sum_a K_a \left(\theta_{ijk} - \theta_{ijk,0}\right)^2 + \cdots \\ &\cdots \frac{1}{2}\sum_t \left(K_1\left(1+\cos\phi_{ijkl}\right) + K_2\left(1-\cos 2\phi_{ijkl}\right) + \cdots\right. \\ &\left.\cdots + K_3\left(1+\cos 3\phi_{ijkl}\right)\right) \end{aligned} \tag{2}$$

Systems were created differently according to the desired calculated property. However, regardless of how the cell was built, all simulations were first relaxed *via* an energy minimisation of the system, followed by a NVT thermalisation to drag the system to the working temperature using the Langevin thermostat (Schneider and Stoll, 1978). When the system is thermally stable, an NVT equilibration was done using the Nosé–Hoover thermostat (Nosé, 1984) to reproduce a proper canonical ensemble. After this equilibration, saturation densities, compositions, pressures and interfacial tensions can be obtained with a direct coexistence simulation. All simulations were time-evolved using a timestep of 1 fs, which is 1/10th of the fastest vibrational mode, as recommended in MD simulations (Braun et al., 2018).

In direct coexistence, the initial configuration was built by placing N molecules in a parallelepiped box of 45 × 45 × 225 Å^3 divided into two symmetric regions to place sensibly large vapour and liquid phases (Müller et al., 2021). When dealing with binary and ternary blends, the box size was increased to 60 × 60 × 300 Å^3 to improve the phase space sampling in mixtures. The number of atoms, N, was set to match the coexistence densities ρ_L and ρ_V at each temperature. The specific number of molecules employed in each specific simulation is compiled in Tables S2 to S4 in the SM. The cell was equilibrated during 50 ns and density, $\rho(z)$, and pressure, $P(z)$, profiles were obtained by averaging the number of molecules and the per-atom stress tensor in 1 Å bins along the z-direction in the last 10 ns window, from where coexistence densities and vapour pressures were obtained,

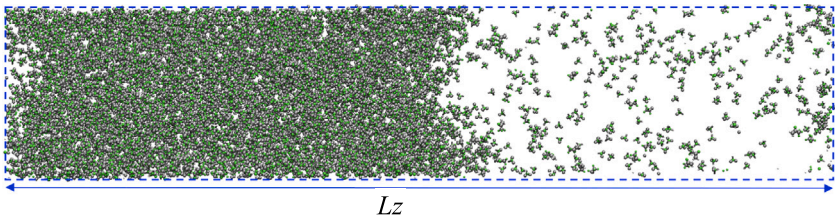

Fig. 2. Configuration of a characteristic vapour-liquid equilibrium simulation.

Table 1
Bibliographic sources for the determination of ideal heat capacities.

System	Type of data	Source
R1234yf	Experimental, correlated	Kano et al. (2010)
R1233zd(E)	Experimental, correlated	Hulse et al. (2012)
R32	Correlated	Outcalt and McLinden (1995)
R125	Correlated (technical report)	EI du Pont de Nemours and Co (2004a)
R134a	Correlated (technical report)	EI du Pont de Nemours and Co (2004b)

respectively. Molecular simulations converged when the density and interfacial tension profiles exhibited time-invariant shapes and each bulk behaved homogeneously (i.e., both properties show a flat plateau). For illustrative purposes, a snapshot of an equilibrated simulation box is shown in Fig. 2. Examples of converged plots are also shared in Fig. S1 of the SM. Finally, by integration of the aforementioned $P(z)$-profile around an interface through the z-direction, the surface tension was obtained directly, following the Irving and Kirkwood formulation shown in Eq. (3) (Irving and Kirkwood, 1950).

$$\gamma = \int_{z_\alpha}^{z_\beta} \left(P_{zz}(z) - \frac{P_{xx}(z) + P_{yy}(z)}{2} \right) dz \tag{3}$$

Heat capacities and viscosities were obtained by building single-phase homogeneous cells for liquids and vapours containing 1500 and 200 molecules, respectively. Volumes of the simulation cells were chosen to match the previously calculated coexistence densities from MD (see Tables S2 to S4 in the SM). Simulations were carried out as 100 ps NPT equilibration, to set the temperature and pressure to the previously calculated saturation condition, and a 1 ns NPT production, both with the Nosé–Hoover thermostat (Nosé, 1984) and Martyna barostat (Martyna et al., 1994), respectively.

Isobaric heat capacities were calculated from the respective ideal and residual contributions, as $C_P = C_P^{\mathrm{id}} + C_P^{\mathrm{r}}$. The former was obtained from bibliographic sources shown in Table 1, whereas the latter was obtained from the slope of the isobaric intermolecular (residual) enthalpy *vs.* temperature ($C_P = (\partial \tilde{H}/\partial T)_P$) of five isobaric NPT simulations at slightly different temperatures (i.e., from $T - 4$ K to $T + 4$ K). The residual enthalpy was estimated by subtracting the kinetic and intramolecular energy from the total enthalpy.

Finally, viscosities were calculated with the Green–Kubo (GK) formalism, displayed in Eq. (4).

$$\eta_{ij} = \beta V \int_0^\infty \langle P_{ij}(t) \cdot P_{ij}(0) \rangle \mathrm{d}t \tag{4}$$

In this framework, a swarm of 100 independent simulations were built and equilibrated as described for the heat capacity procedure. Once equilibrated, thermostats and barostats are turned off during 1 ns to build and integrate the corresponding off-diagonal components, $ij = xy, xz, yz$, of the pressure autocorrelation functions, $\langle P_{ij}(t) \cdot P_{ij}(0) \rangle$. The final viscosity is the average of the three off-diagonal integrals over the 100 runs. Additionally, the large noise in the integral of Eq. (4) has been treated by using the time-decomposition method (Zhang et al., 2015). Characteristic autocorrelation functions, their Green–Kubo integration and time limit found by the time-decomposition method are illustrated in Fig. S2 of the SM.

2.2. Refrigerant modelling

The soft-SAFT equation of state (Blas and Vega, 1997) is a variant of the original SAFT equation (Chapman et al., 1989, 1990) based on a reference LJ potential (Lennard-Jones, 1931), which accounts for both repulsive and dispersive contributions simultaneously using the Johnson's EOS for the LJ monomers and chains (Johnson et al., 1993, 1994). Soft-SAFT is written as a sum of microscopic contributions to the total residual Helmholtz free energy. For the particular case of the studied fluorinated refrigerants, whose nature has a significant dipole moment, these contributions include the interactions among segments, the formation of chains from identical segments, and the polar forces,

$$\tilde{a}^{\mathrm{r}} = \tilde{a} - \tilde{a}^{\mathrm{i}} = \tilde{a}^{\mathrm{ref}} + \tilde{a}^{\mathrm{ch}} + \tilde{a}^{\mathrm{p}}, \tag{5}$$

where the superscripts i, ref, ch, and p refer to the ideal, reference, chain, and polar contributions, respectively.

The reference term is a LJ spherical fluid, defined by two molecular parameters: the segment diameter, σ_{ii}, and the dispersive energy between two LJ monomers, ε_{ii}, while the chain term is defined by a characteristic length, m_i. These contributions have been widely described in the literature and the reader is referred to the original works (Johnson et al., 1993, 1994; Blas and Vega, 1997) for the mathematical structure.

The polar term has been explicitly considered for an accurate description of the dipole moment (Alkhatib et al., 2020; Albà et al., 2021), and it is based on the multipolar expression of Gubbins and Twu (1978) and Twu and Gubbins (1978) for spherical molecules using the Padé approximation of Stell and coworkers (Stell et al., 1972), as

$$\tilde{a}^{\mathrm{p}} = \frac{a_2}{1 - a_3/a_2}, \tag{6}$$

where a_2 and a_3 are the second and third-order terms in the Padé expansion related to two and three-body interactions. Each polar moment is associated with two additional molecular parameters, the fraction of polar segments $x_{\mathrm{p}i}$ and the dipole moment, μ_{ii}. The details of the expansion can be seen in the application of Alkhatib and Vega (2021). The quantitative values of the five parameters for each compound are taken from literature and shown in Table 2.

The extension of the theory to mixtures is performed by applying the van der Waals one-fluid theory (Waals, 1891) to the modified Berthelot combining rule (Berthelot, 1898), as

$$\sigma_{ij} = \frac{\sigma_{ii} + \sigma_{jj}}{2} \tag{7}$$

$$\varepsilon_{ij} = \xi_{ij} \left(\varepsilon_{ii} \varepsilon_{jj} \right)^{1/2}, \tag{8}$$

where ξ_{ij} is the Berthelot energy binary parameter, commonly used to correct deviations from the mean dispersive energy value, as a consequence of the complex interactions between both fluids. This binary interaction parameter had been fitted to REFPROP data in a previous contribution (Albà et al., 2023b) to accurately describe the vapour-liquid equilibria of binary systems, and is reported in Table 3 for completeness. Being temperature and composition independent, it can be applied to any mixture containing the two studied compounds, regardless of the content. In addition, ternary blends are predicted from the information obtained for the binary pairs.

Table 2
Soft-SAFT molecular parameters[a] and free-volume theory parameters for the pure compounds of this work.

	M_w g mol^{-1}	m_i	σ_{ii} Å	ϵ_{ii}/k_B K	μ_{ii} C m	x_{pi}	$L_v \cdot 10^{11}$ Å	$B \cdot 10^2$	α [b]	AAD_{FTV} pph
R1234yf	114.00	1.740	4.082	191.6	6.70790	0.70	8.31	1.560	24.13	0.98
R1233zd(E)	130.50	2.331	3.819	232.6	3.81190	0.80	9.61	1.476	25.88	0.96
R32	52.02	1.376	3.506	164.5	6.59790	0.75	8.04	1.350	20.29	5.22
R125	120.02	1.887	3.790	165.1	5.21360	0.90	8.90	1.350	20.51	3.28
R134a	102.01	1.813	3.770	169.5	6.86475	0.70	11.35	1.350	20.29	6.09

[a] Soft-SAFT parameters are taken from previous contribution (Albà et al., 2021) while FVT parameters are obtained in this work fitting to REFPROP data (Lemmon et al., 2018).
[b] α in J m^3 mol^{-1} kg^{-1}.

Table 3
Energy binary interaction parameter, ξ_{ij}, between the selected refrigerants. A value of 1.000 indicates that no adjustment is necessary (Albà et al., 2023b).

	R1234yf	R32	R125	R134a
R1234yf	–	0.970	1.000	0.983
R32	–	–	0.985	0.980
R125	–	–	–	0.993
R134a	–	–	–	–

Table 4
Influence parameters for the DGT fitted using correlated REFPROP data (Lemmon et al., 2018).

	$a \cdot 10^{24}$ K^{-2}	$b \cdot 10^{22}$ K^{-1}	$c \cdot 10^{19}$	T_{min} K	T_{max} K
R1234yf	0.000	−9.490	3.890	250.00	350.00
R1233zd(E)	0.000	−6.260	3.900	260.00	400.00
R32	−1.190	4.880	−0.132	180.00	320.00
R125	−4.890	21.600	−1.320	220.00	310.00
R134a	−3.080	13.900	−0.562	240.00	340.00

The interfacial tension of the studied refrigerants has been modelled using the density gradient theory (DGT) obtained from the work of Cahn and Hilliard (1958), rooted in the theory of van der Waals for inhomogeneous fluids (van der Waals, 1894). In this approach, the expression for the Helmholtz free energy is expanded in a Taylor series around the free energy density term of the homogeneous fluid at the local density and truncated after the second-order term. The mathematical shape of the DGT yields

$$A = \int \left(a_0(\rho) + \frac{1}{2} \sum_i \sum_j c_{ij} \nabla\rho_i \nabla\rho_j \right) \mathrm{d}^3 r, \tag{9}$$

where $\nabla\rho_x$ is the local gradient in the density of a component $x = i, j$. An influence parameter, c_{ij}, is defined to treat the phenomenological behaviour as a parameter fitted to correlated REFPROP surface tension data (Lemmon et al., 2018). The influence parameters are fitted using a polynomial form given by

$$c_{ii} = aT^2 + bT + c \tag{10}$$

The parameters for Eq. (10) are shown in Table 4 and the influence parameters for mixtures are obtained through a geometric average, without further fitting.

For a planar interface, and assuming that the density dependence of the influence parameter can be neglected, functional minimisation of Eq. (9) for phase coexistence conditions leads to

$$\gamma = \sum_i \sum_j \int_{-\infty}^{\infty} c_{ij} \frac{\mathrm{d}\rho_i}{\mathrm{d}z} \frac{\mathrm{d}\rho_j}{\mathrm{d}z} = 2 \int_{-\infty}^{\infty} \left(a_0(\rho) - \sum_i \rho_i \mu_{0i} - P_0 \right) \mathrm{d}z, \tag{11}$$

where μ_{0i} and P_0 are the equilibrium chemical potential and pressure, respectively, and z is the perpendicular vector to the interface. For additional details on the implementation of the theory, the reader is referred to previous contributions (Duque et al., 2004; Mejía and Segura, 2004).

Finally, the description of the viscosity is carried out by coupling the free-volume theory (FVT) into soft-SAFT. The FVT is an approach proposed and detailed by Allal et al. (2001a,b), where the viscosity, η, is obtained from the sum of a diluted, η_0, and dense contributions, $\Delta\eta$, i.e., $\eta = \eta_0 + \Delta\eta$. The diluted viscosity comes from the Chung's application (Chung et al., 1988) of the Chapman–Enskog (Chapman, 1916) theory, and reads

$$\eta_0 = \kappa \frac{\sqrt{M_w T}}{\tilde{v}_c^{2/3} \Omega} F_c, \tag{12}$$

where M_w is the molecular weight in g mol^{-1}, T is the thermodynamic temperature, and $\tilde{v}_c$ is the critical molar volume in L mol^{-1}. F_c and Ω are dimensionless values, being F_c an empirically determined correction and Ω the reduced collision integral. Additionally, $\kappa = 4.07804 \cdot 10^{-8}$ yields the diluted viscosity in Pa s. All thermodynamic values are obtained from the EOS to preserve the results' homogeneity.

Furthermore, the dense contribution is given by

$$\frac{\Delta\eta}{L_v} = \Phi \left(\frac{M_w}{3RT} \right)^{1/2} \exp\left(\left(B \frac{\Phi}{RT\rho} \right)^{3/2} \right), \tag{13}$$

where P is the absolute pressure, ρ the density, R is the universal gas constant, and $\Phi = P + \alpha\rho^2 M_w$. This term involves three fitted parameters related to free-volume overlap, B, energy, α, and structural effects, L_v, whose values have been fitted using viscosity experimental data, and are also included in Table 2.

3. Pure refrigerant

This study provides a comprehensive theoretical framework to evaluate a series of essential thermophysical properties of common refrigerants. It focuses on three standard HFCs (R32, R125, and R134a) and two 4th-generation HFOs (R1234yf and R1233zd(E)). The selected refrigerants are the basis for various blends. Initially, MD simulations have been used to reproduce the vapour-liquid equilibrium, interfacial tension, heat capacity, and viscosity of these compounds. For this purpose, three different temperatures are evaluated along the saturation line to check the predictive capabilities of the selected force fields. Simulations close to the critical point are not performed to avoid errors in calculating equilibrium properties. The results are graphically summarised in Fig. 3 and numerically displayed in Table S5 of the SM. Before assessing against experimental data, the MD simulations were validated by comparing the available results against Grand Canonical Monte Carlo (GCMC) simulations reported in previous literature (Raabe and Maginn, 2010a; Peguin et al., 2009; Raabe, 2013, 2015). As shown in Figure S3 of the SM, this comparison demonstrates excellent agreement between both datasets, despite the differences in simulation techniques.

The REFPROP database (blue dotted lines) is used for comparison with the MD results (crimson symbols) for all the properties of the pure fluids to corroborate their accuracy. MD predictions completely match both the saturated densities (Fig. 3a) and vapour pressure (Fig. 3b) of all fluids, with a minor discrepancy for R32 at the highest temperature. It is important to notice that the highest temperature

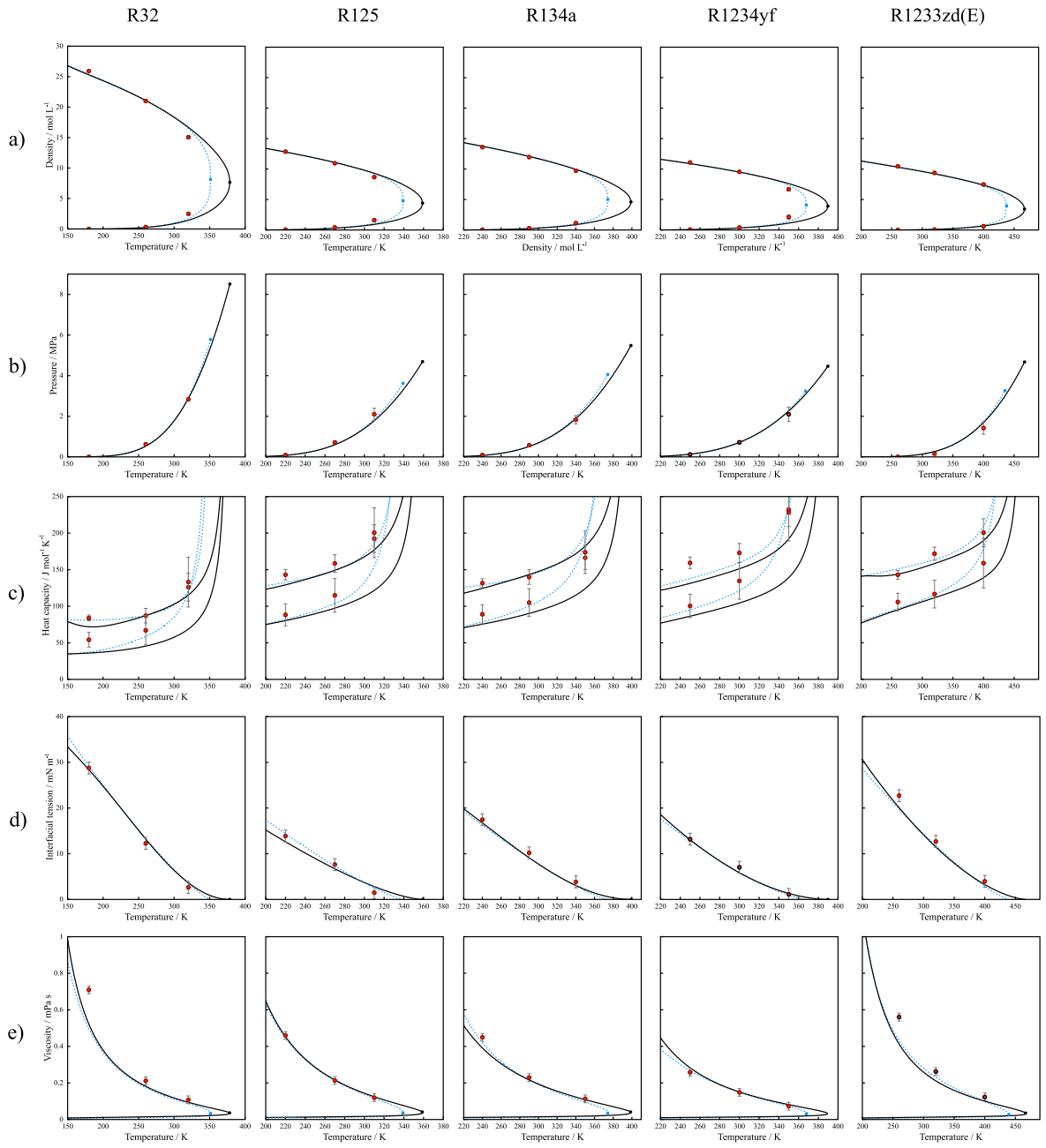

Fig. 3. (a) Vapour-liquid coexistence curves, (b) Vapour pressures, (c) Saturated liquid (top) and vapour (bottom) heat capacities, (d) Interfacial tensions, and (e) Saturated liquid viscosities for R32, R125, R134a, R1234yf, and R1233zd(E). Crimson symbols represent MD simulation results, blue dotted lines are REFPROP data, and solid lines are soft-SAFT calculations. Error bars are added in all MD cases. For interpretation of the references to colour in this figure legend, the reader is referred to the web version of this article.

of this refrigerant is close to the critical region and may suffer from its inherent inhomogeneous behaviour, exhibiting higher inaccuracies. Still, the results of the MD simulations allow a good description of the system. The rendering of the heat capacity is of particular interest because this is a second-order derivative property that is not used in the fitting of the force fields and is more challenging to describe. However, excellent agreement is observed in most fluids (Fig. 3c), even though the uncertainty of the calculation is higher than for the previous properties, as can be noticed from the error bars. The MD simulations slightly overpredict the heat capacity in both phases, with R1234yf displaying the highest deviations.

Regarding surface tension, the results align perfectly with the REFPROP data (Fig. 3d). The most significant deviations occur with R1233zd(E), likely due to the presence of a chlorine atom in its composition. Finally, the viscosity results are also remarkable (Fig. 3e) in all cases, reinforcing the validity of the model. MD results are fully predictive, as no data for transport properties has been used by Raabe (2015, 2017, 2020) to correlate the force field.

Once the MD data have been validated, showing that a common and consistent molecular framework allows the description of various properties, the soft-SAFT EOS is added as a second modelling tool to the study. The EOS results are displayed in continuous lines in Fig. 3. As expected, an excellent description of the phase envelope is achieved with the soft-SAFT model, provided that the molecular parameters of Table 2 were fitted to the REFPROP data. However, the description of the heat capacity in Fig. 3c is a key factor in evaluating the predictive ability of the method. The heat capacity is a highly temperature-sensitive and second-order derivative property, not used when fitting the soft-SAFT molecular parameters. While the qualitative results are promising, soft-SAFT slightly underestimates the

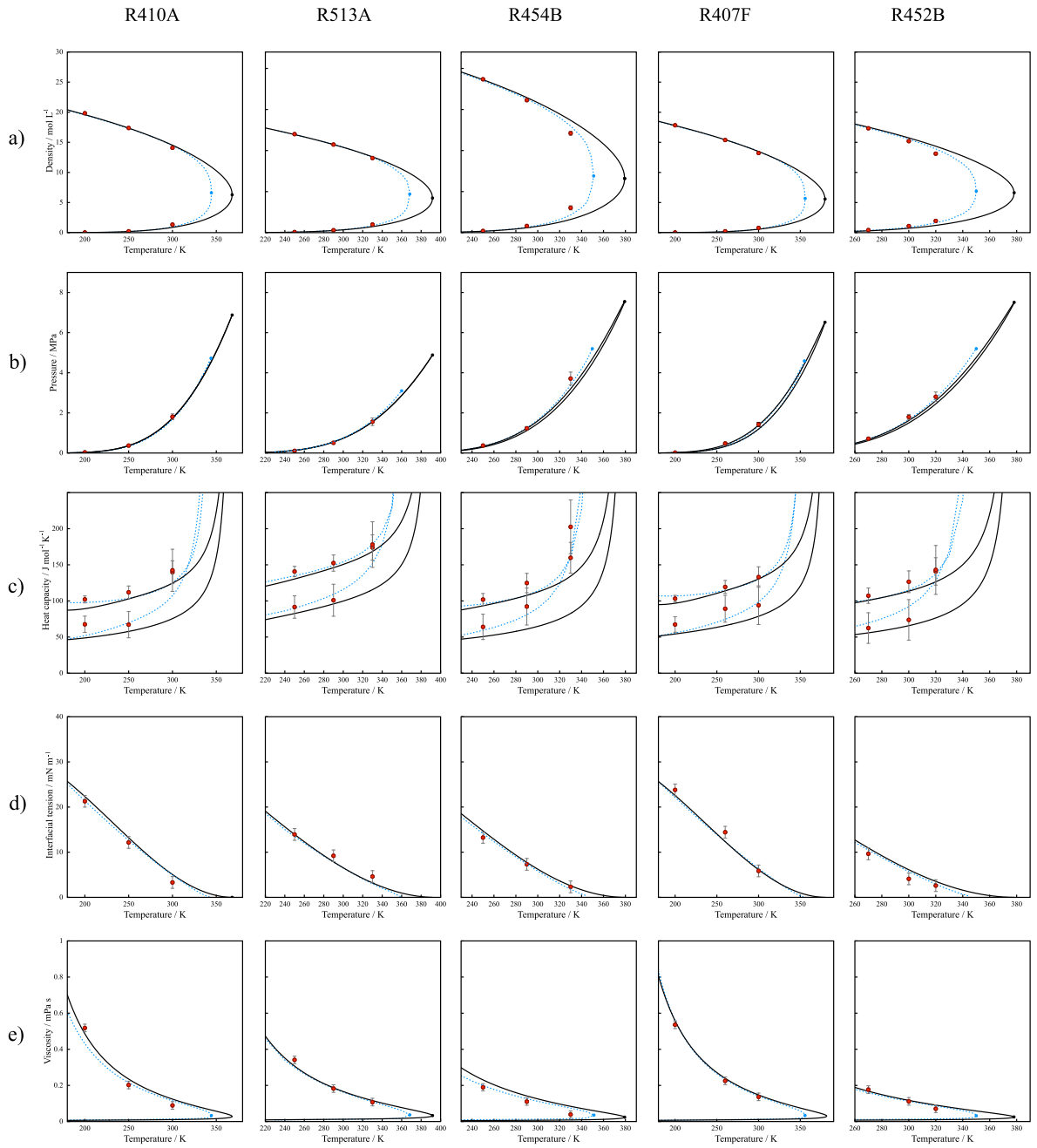

Fig. 4. (a) Vapour-liquid coexistence curves of binary and ternary blends, (b) Vapour pressures, (c) Saturated liquid (top) and vapour (bottom) heat capacities, (d) Interfacial tensions, and (e) Saturated liquid viscosities for R410A, R513A, R454B, R407F, and R452B. Crimson symbols represent MD simulation results, blue dotted lines are REFPROP data, and solid lines are soft-SAFT calculations. Error bars are added in all MD cases. For interpretation of the references to colour in this figure legend, the reader is referred to the web version of this article.

values of this property in both phases compared to MD simulations and REFPROP data. The deviation increases at higher temperatures, likely due to the overestimation of the critical point inherent to the application of a mean-field theory. These discrepancies in the critical area can be overcome by introducing a specific crossover treatment that considers the inherent fluctuations near the critical zone (Llovell and Vega, 2007). Nonetheless, this is out of the scope of this work since the operation conditions for refrigerants are far from this point.

Following with the surface tension, the EOS performance is excellent, as seen in Fig. 3(d). However, it must be noted that the influence parameter, c_{ii}, has been fitted for the DGT theory, facilitating this agreement. Similarly, the free-volume theory (FVT) integrated into the soft-SAFT EOS can perfectly reproduce the REFPROP data, as seen in Fig. 3e, even at low temperatures, using the fitted parameters presented in Table 2.

These modelling results represent the first necessary step before extending the theoretical framework to blends, where the capabilities of MD simulations and soft-SAFT can be better appreciated. The following section will highlight this fact, showing the practical applications of this research and its potential to influence in the design of new refrigerants through thermophysical characterisation.

4. Refrigerant blends

Following a similar structure to that shown for the pure refrigerants, the main thermophysical properties of three binary (R410A, R513A,

and R452B) and two ternary blends (R407F and R454B) have been studied. Molecular Dynamics are compared to REFPROP correlated data (Lemmon et al., 2018) and the soft-SAFT modelling, as presented in Fig. 4.

Overall, excellent agreement is found between the MD simulations and REFPROP, confirming the validity of the method to predict the properties of blends without experiencing a degeneration in the description. The prediction of the saturated densities and vapour pressures is excellent, with some minor deviations at the highest temperature of R452B and R454B as a consequence of the vicinity of the critical region. Remarkably, the description of the heat capacity is also excellent, although the MD simulations slightly overestimate the values compared to REFPROP. Nevertheless, all results are within the error range. Finally, no remarkable differences with the correlated data are found for the interfacial tension and the viscosity, with a minor deviation at the low-temperature value of R410A.

Moreover, the comparison with the soft-SAFT modelling also offers a very good description of all properties. Density and vapour pressure are accurately described, while the soft-SAFT prediction of the isobaric vapour heat capacity is smaller in all cases. Still, these values are within the same uncertainty range than those of pure compounds. Interfacial tension and viscosity also display an excellent performance, being capable to predict the experimental behaviour in the whole phase envelope.

It is important to note that the application of the polar contribution in the soft-SAFT EOS is advantageous for a more meaningful description of the thermophysical properties of pure refrigerants and blends, as it can be noticed from the excellent prediction of ternary systems. The polar term provides flexibility to the soft-SAFT structure and a better performance fitting saturation densities at high temperatures and predicting the heat capacity, while maintaining similar results for the rest of properties. The lack of the polar term results in a deterioration of the capability to extrapolate the thermophysical properties to other systems and conditions, being unsuitable to be utilised as a predictive tool.

4.1. Low-temperature refrigerants

Based on the previous results, it is possible to conduct a thermodynamic analysis to compare the technical properties of the different refrigerants. This subsection considers low-temperature refrigerants, including working fluids with a cooling capacity to work in refrigeration applications below zero Celsius degrees (note that this is an empirical taxonomy, which depends on their final application Xiao et al., 2023).

This comparison involves R407F (GWP = 1965), one of the most common commercial blends, R134a (GWP = 1530), adequate for a wide range of applications, and R513A, which is a mid-GWP (GWP = 673.5) alternative azeotropic mixture, whose glide temperature is considered negligible, as seen in the corresponding frame for pressure in Fig. 5. This refrigerant is sold under the OPTEON^{TM} brand to replace R134a in positive displacement, direct expansion, medium and low-temperature commercial and industrial chillers, and flooded or centrifugal chillers. As R134a, ASHRAE classifies R513A as a nontoxic and nonflammable fluid (A1).

Fig. 5 compares three essential properties, vapour pressure, interfacial tension, and viscosity, of these refrigerants to evaluate the suitability of R134a and R513A as replacements for R407F. In terms of vapour pressure, the differences between R134a and R513A are negligible, as shown in Fig. 5(a). However, both have lower values compared to R407F, which could allow lower condenser pressures in a refrigeration cycle, potentially resulting in slight energy savings. Regarding interfacial tension, R513A performs similarly to R407F, while pure R134a exhibits higher values, as depicted in Fig. 5(b). In this context, a lower interfacial tension is preferable because it facilitates heat transfer during the isobaric stages of a refrigeration cycle by reducing droplet formation, increasing wettability and entrainment. Moreover, droplet formation would also impact the expansion stage in organic Rankine cycles, especially in fluids with wet behaviour (González et al., 2022, 2023b). Finally, Fig. 5(c) illustrates the differences in viscosity. Once again, R134a shows a higher viscosity, while R513A and R407F exhibit similar performance, which is more favourable for reducing energy consumption due to fluid flow within the system.

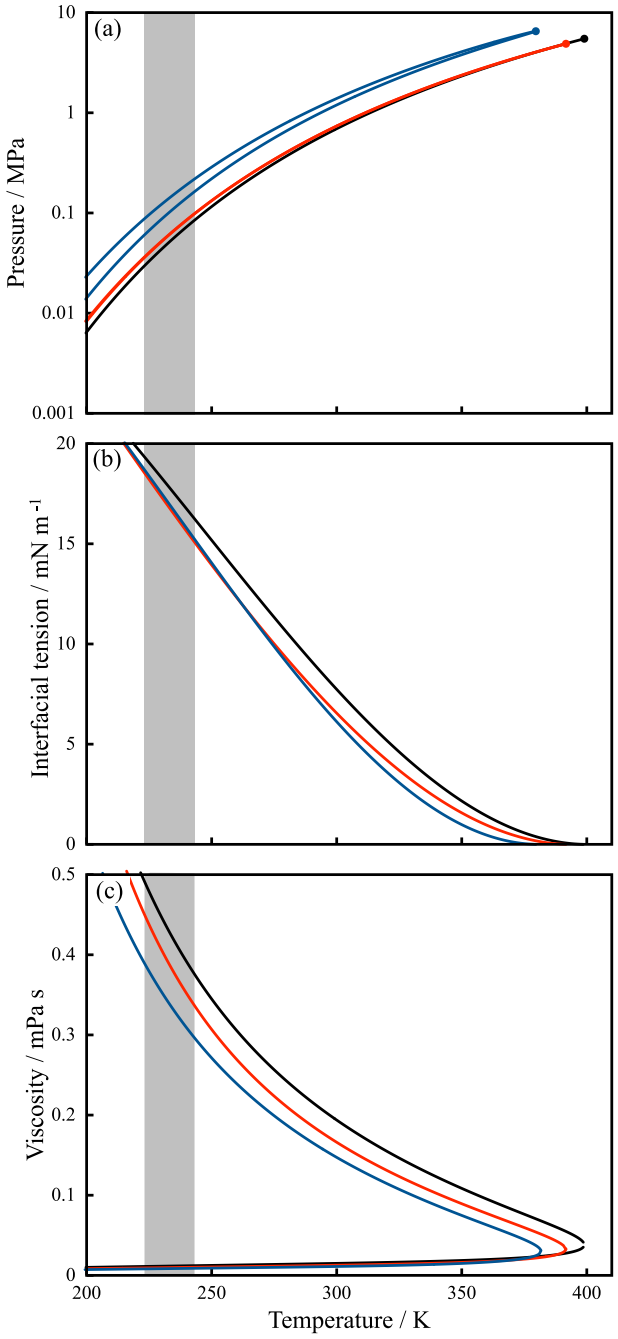

Fig. 5. Comparison of the (a) Vapour pressure, (b) Interfacial tension, and (c) Viscosity of three low-temperature refrigerants as predicted by soft-SAFT. R134a in black, R513A in crimson, and R407F in blue. The shaded area is the usual temperature range of low-temperature refrigerants from 223.15 to 243.15 K. For interpretation of the references to colour in this figure legend, the reader is referred to the web version of this article.

Considering all three properties, R513A emerges as a good and feasible alternative, offering lower vapour pressure and similar interfacial tension and viscosity than R407F, but with a much lower GWP.

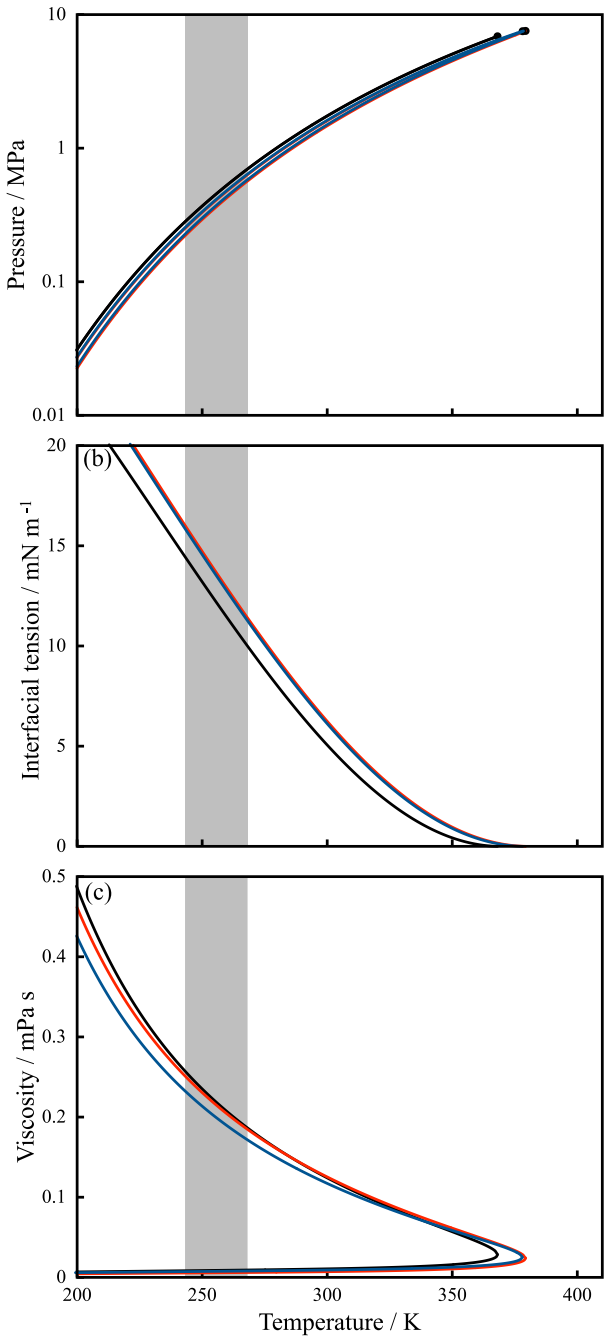

Fig. 6. Comparison of the (a) Vapour pressure, (b) Interfacial tension, and (c) Viscosity of three mid-temperature refrigerants as predicted by soft-SAFT. R410A in black, R454B in crimson, and R452B in blue. The shaded area is the usual temperature range of mid-temperature refrigerants from 243.15 to 268.15 K. For interpretation of the references to colour in this figure legend, the reader is referred to the web version of this article.

4.2. Mid-temperature refrigerants

The second group of refrigerants comprises those within a mid-temperature range, generally employed for air-cooling and thermally-activated refrigeration cycles (González et al., 2023a). R410A (GWP = 2500) is the dominant refrigerant in residential heat pumps. Two mid-GWP refrigerants are proposed here as potential replacements: R452B (GWP = 676) and R454B (GWP = 466), originally named DR55 and DR5A, respectively. R452B is sold under the OPTEON^{TM} brand as a replacement for R410A. It comprises a mixture of R32, R125, and R1234yf in a 67/7/26 wt% ratio and is classified as a mildly-flammable refrigerant (A2L). R454B, on the other hand, is a binary mixture of R32 and R1234yf in a 68.9/31.1 wt% ratio and is also classified as an A2L refrigerant. These working fluids are indicated for usage in residential and commercial positive displacement devices, direct expansion (DX) chillers and air conditioning (AC) applications.

The technical comparison between these three blends of refrigerants is provided in Fig. 6, in a similar manner as done for the low-temperature refrigerants in Section 4.1. The analysis reveals a very similar vapour pressure for the three systems (see Fig. 6(a)), even though the two proposed alternatives have very slightly lower values. However, the interfacial tension of R454B and R452B is almost identical, but higher than R410A, as seen in Fig. 6(b), while the viscosity of the new blends is slightly lower except in the near critical region (see Fig. 6(c)), favouring the system in terms of energy cost. Consequently, no significant differences have been found among the three mid-temperature blends, with R452B and R454B exhibiting identical properties, being slightly worse in terms of interfacial tension and slightly better in terms of viscosity, compared to R410A. These minor differences do not represent, however, a constraint in considering the replacement of R410A, given the significant decrease in terms of GWP of the new systems.

5. Conclusions

This work has used two complementary modelling tools, molecular dynamics and an equation of state (soft-SAFT EOS), to carry out a comprehensive thermophysical description of five pure refrigerants and five commercial blends based on these pure compounds. For this purpose, an accurate force field, available in the literature, was used to perform MD simulations at three different temperatures to determine the saturated density, vapour pressure, heat capacity, interfacial tension and viscosity at equilibrium conditions for all systems. The new results were compared with available correlated data from REFPROP, displaying good agreement in all cases. Further to this validation, the molecular-based soft-SAFT EOS, coupled with the Free-Volume and Density Gradient theories, was used to describe all these properties in the entire phase envelope, allowing quick and reliable predictions at different conditions.

Based on the thermophysical variables evaluated, a preliminary technical assessment was conducted to compare possible substitutes for the high GWP refrigerant blends R407F and R410A. R513A is presented as a physically reliable alternative for the former, provided its similar vapour pressure and lower interfacial tension and viscosity, favouring heat transfer and flow movement. For the latter, no significant differences were appreciated regarding thermodynamic properties, with similar vapour pressure and viscosity and very minor differences in interfacial tension. Otherwise, this ensures a comparable performance of R452B and R454B, an excellent option for replacing R410A, given their lower GWP.

Overall, this work highlights the complementarity between MD simulations and theoretical EOSs with a specific polar contribution. While MD provides access to previously unknown data, soft-SAFT coarse-grained models retain essential molecular information to reproduce these thermophysical properties and extend calculations to novel mixtures. This allows for a rapid qualitative screening of multiple options, identifying the most promising blends efficiently.

CRediT authorship contribution statement

Daniel Jovell: Software, Investigation, Conceptualization. **Gerard Alonso:** Writing – original draft, Investigation. **Pablo Gamallo:** Validation, Methodology. **Rafael Gonzalez-Olmos:** Writing – review & editing, Supervision. **Héctor Quinteros-Lama:** Writing – review & editing, Supervision, Project administration. **Fèlix Llovell:** Writing – review & editing, Supervision, Funding acquisition, Formal analysis.

Declaration of competing interest

The authors declare that they have no known competing financial interests or personal relationships that could have appeared to influence the work reported in this paper.

Acknowledgements

This research is supported by project NEW-F-TECH (TED2021-130959B-I00) funded by the Spanish Ministry of Science and Innovation MICIU/AEI/10.13039/-501100011033/ and the European Union Next Generation-EU/-PRTR. Additional support from MICIU/AEI/10.13039/-501100011033/ from projects STOP-F-Gas (PID 2019-108014RB-C21), REFCICLA (PID2023-149713OB-I00) and ZEO4GREEN (PID2022-138180OB-I00) is appreciated. P.G. acknowledges project CEX2021-01202-M María de Maeztu Unit of Excellence, also funded by MICIU/AEI/10.13039/-501100011033/ and ERDF A way of making Europe/-PRTR. H.Q.-L. and G.A. acknowledge funding from FONDECYT, Chile, under projects no. 1240765 and 11230012, respectively. H.Q.-L. is also grateful for the support of FOVI220054. Additional funding from the European Union, Next Generation EU within the framework of the Recovery, Transformation, and Resilience Plan "Investigo Program" for the hiring of young job seekers for the development and execution of research and innovation functions, tasks, and initiatives is acknowledged. Recognition from AGAUR as Consolidated Research Groups for GESPA (2021 SGR 00321), AGACAPE (SGR 2021 00738) and CMSL (2021 SGR 00079) is gratefully appreciated. Finally, authors thank to the CSUC and Red Española de Supercomputación (RES) for the supercomputing time granted.

Appendix A. Supplementary data

The Supplementary Material contains details of the force fields, the parameters for the cell initiation, examples of the calculation and viscosity calculations' convergence, and, finally, the numerical data of the MD simulations.

Supplementary material related to this article can be found online at https://doi.org/10.1016/j.ijrefrig.2025.03.026.

References

Aasen, A., Hammer, M., Ervik, A., Müller, E.A., Wilhelmsen, O., 2019. Equation of state and force fields for feynman–hibbs-corrected mie fluids, i. application to pure helium, neon, hydrogen, and deuterium. J. Chem. Phys. 151 (6), 064508. http://dx.doi.org/10.1063/1.5111364.

Al Ghafri, S.Z., Rowland, D., Akhfash, M., Arami-Niya, A., Khamphasith, M., Xiong, X., Tsuji, T., Tanaka, Y., Seiki, Y., May, E.F., Hughes, T.J., 2019. Thermodynamic properties of hydrofluoroolefin (r1234yf and r1234ze(e)) refrigerant mixtures: Density, vapour-liquid equilibrium, and heat capacity data and modelling. Int. J. Refrig. 98, 249–260. http://dx.doi.org/10.1016/j.ijrefrig.2018.10.027.

Albà, C.G., Alkhatib, I., Llovell, F., Vega, L.F., 2021. Assessment of low global warming potential refrigerants for drop-in replacement by connecting their molecular features to their performance. ACS Sustain. Chem. Eng. 9 (50), 17034–17048. http://dx.doi.org/10.1021/acssuschemeng.1c05985.

Albà, C., Alkhatib, I., Llovell, F., Vega, L., 2023a. Hunting sustainable refrigerants fulfilling technical, environmental, safety and economic requirements. Renew. Sustain. Energy Rev. 188, 113806. http://dx.doi.org/10.1016/j.rser.2023.113806.

Albà, C., Alkhatib, I., Llovell, F., Vega, L., 2023b. Hunting sustainable refrigerants fulfilling technical, environmental, safety and economic requirements. Renew. Sustain. Energy Rev. 188, 113806. http://dx.doi.org/10.1016/j.rser.2023.113806.

Alkhatib, I., Pereira, L.M.C., Torne, J., Vega, L.F., 2020. Polar soft-SAFT: theory and comparison with molecular simulations and experimental data of pure polar fluids. Phys. Chem. Chem. Phys. 22 (23), 13171–13191. http://dx.doi.org/10.1039/D0CP00846J.

Alkhatib, I., Vega, L.F., 2021. Quantifying the effect of polar interactions on the behavior of binary mixtures: Phase, interfacial, and excess properties. J. Chem. Phys. 154 (16), 164503. http://dx.doi.org/10.1063/5.0046034.

Allal, A., Boned, C., Baylaucq, A., 2001a. Free-volume viscosity model for fluids in the dense and gaseous states. Phys. Rev. E 64 (1), 011203. http://dx.doi.org/10.1103/PhysRevE.64.011203.

Allal, A., Moha-ouchane, M., Boned, C., 2001b. A new free volume model for dynamic viscosity and density of dense fluids versus pressure and temperature. Phys. Chem. Liq. 39 (1), 1–30. http://dx.doi.org/10.1080/00319100108030323.

2016. Amendment to the Montreal Protocol on Substances that Deplete the Ozone Layer. European Parliament and Council.

Arp, H.P.H., Gredelj, A., Glüge, J., Scheringer, M., Cousins, I.T., 2024. The global threat from the irreversible accumulation of trifluoroacetic acid (tfa). Environ. Sci. Technol. 58 (45), 19925–19935. http://dx.doi.org/10.1021/acs.est.4c06189.

Asensio-Delgado, S., Jovell, D., Zarca, G., Urtiaga, A., Llovell, F., 2020. Thermodynamic and process modeling of the recovery of R410A compounds with ionic liquids. Int. J. Refrig. 118, 365–375. http://dx.doi.org/10.1016/j.ijrefrig.2020.04.013.

Befort, B.J., DeFever, R.S., Maginn, E.J., Dowling, A.W., 2022. Machine learning-enabled optimization of force fields for hydrofluorocarbons. Comput. Aided Chem. Eng. 49, 1249–1254. http://dx.doi.org/10.1016/B978-0-323-85159-6.50208-6.

Befort, B.J., DeFever, R.S., Tow, G.M., Dowling, A.W., Maginn, E.J., 2021. Machine learning directed optimization of classical molecular modeling force fields. J. Chem. Inf. Model. 61 (9), 4400–4414. http://dx.doi.org/10.1021/acs.jcim.1c00448.

Berthelot, D., 1898. Sur le mélange des gaz. C. R. Hebd. Séances Acad. Sci. 126 (1), 1703–1706.

Blas, F.J., Vega, L.F., 1997. Thermodynamic behaviour of homonuclear and heteronuclear lennard-jones chains with association sites from simulation and theory. Mol. Phys. 92 (1), 135–150. http://dx.doi.org/10.1080/002689797170707.

Braun, E., Gilmer, J., Mayes, H.B., Mobley, D.L., Monroe, J.I., Prasad, S., Zuckerman, D.M., 2018. Best practices for foundations in molecular simulations [article v1.0]. Living J. Comput. Mol. Sci. 1 (1), 5957. http://dx.doi.org/10.33011/livecoms.1.1.5957.

Burkholder, J.B., Cox, R.A., Ravishankara, A.R., 2015. Atmospheric degradation of ozone depleting substances, their substitutes, and related species. Chem. Rev. 115 (10), 3704–3759.

Cahn, J.W., Hilliard, J.E., 1958. Free energy of a nonuniform system, I. Interfacial free energy. J. Chem. Phys. 28 (2), 258–267. http://dx.doi.org/10.1063/1.1744102.

Chapman, S., 1916. On the law of distribution of molecular velocities, and on the theory of viscosity and thermal conduction, in a non-uniform simple monatomic gas. Philos. Trans. R. Soc. Lond. Ser. A: Math. Phys. Eng. Sci. 216, 279–348. http://dx.doi.org/10.1098/rsta.1916.0006.

Chapman, W.G., Gubbins, K.E., Jackson, G., Radosz, M., 1989. SAFT: equation-of-state solution model for associating fluids. Fluid Phase Equilib. 52 (1), 31–38.

Chapman, W.G., Gubbins, K.E., Jackson, G., Radosz, M., 1990. New reference equation of state for associating liquids. Ind. Eng. Chem. Res. 29 (8), 1709–1721. http://dx.doi.org/10.1021/ie00104a021.

Chung, T., Ajlan, M., Lee, L., Starling, K.E., 1988. Generalized multiparameter correlation for nonpolar and polar fluid transport properties. Ind. Eng. Chem. Res. 27 (4), 671–679. http://dx.doi.org/10.1021/IE00076A024.

Costa Cabral, B.J., Guedes, R.C., Pai-Panandiker, R.S., Nieto de Castro, C.A., 2001. Hydrogen bonding and the dipole moment of hydrofluorocarbons by density functional theory. Phys. Chem. Chem. Phys. 3, 4200–4207. http://dx.doi.org/10.1039/B102879K.

Demirbek, M.G., Rodriguez Reartes, S.B., Llovell, F., 2024. Thermodynamic analysis of the absorption of common refrigerants in fluorinated deep eutectic solvents. Fluid Phase Equilib. 581, 114077. http://dx.doi.org/10.1016/j.fluid.2024.114077.

Duque, D., Pàmies, J.C., Vega, L.F., 2004. Interfacial properties of lennard-jones chains by direct simulation and density gradient theory. J. Chem. Phys. 121 (22), 11395–11401. http://dx.doi.org/10.1063/1.1818679.

Duque, D., Vega, L.F., 2004. Some issues on the calculation of interfacial properties by molecular simulation. J. Chem. Phys. 121 (17), 8611. http://dx.doi.org/10.1063/1.1802672.

EI du Pont de Nemours and Co, 2004a. Thermodynamic Properties of HFC-125. Tech. Rep. du Pont.

EI du Pont de Nemours and Co, 2004b. Thermodynamic Properties of HFC-134a. Tech. Rep. du Pont.

Fermeglia, M., Ferrone, M., Pricl, S., 2003. Development of an all-atoms force field from ab initio calculations for alternative refrigerants. Fluid Phase Equilib. 210 (1), 105–116. http://dx.doi.org/10.1016/S0378-3812(03)00165-1.

Frisch, M., Trucks, G., et al., 2016. Gaussian 16, Revision c.01.

Gao, N., Chen, G., Tang, L., 2018. A corresponding state equation for the prediction of isobaric heat capacity of liquid hfc and hfo refrigerants. Fluid Phase Equilib. 456, 1–6. http://dx.doi.org/10.1016/j.fluid.2017.08.015.

González, J., Garrido, J.M., Quinteros-Lama, H., 2023a. Analysis of the maximum efficiency and the maximum net power as objective functions for organic rankine cycles optimization. Entropy 25 (6), http://dx.doi.org/10.3390/e25060882.

González, J., Llovell, F., Garrido, J.M., Quinteros-Lama, H., 2022. A rigorous approach for characterising the limiting optimal efficiency of working fluids in organic rankine cycles. Energy 254, 124191. http://dx.doi.org/10.1016/j.energy.2022.124191.

González, J., Llovell, F., Garrido, J.M., Quinteros-Lama, H., 2023b. A study of the optimal conditions for organic rankine cycles coupled with vapour compression refrigeration using a rigorous approach based on the helmholtz energy function. Energy 285, 129554. http://dx.doi.org/10.1016/j.energy.2023.129554.

González-Barramuño, B., Cea-Klapp, E., Cerda, S., Polishuk, I., Piñeiro, M.M., Quinteros-Lama, H., Garrido, J.M., 2023. Scaling theories for predicting the viscosity of binary and ternary refrigerant mixtures. Int. J. Refrig. 155, 73–80. http://dx.doi.org/10.1016/j.ijrefrig.2023.07.020.

González-Barramuño, B., Cea-Klapp, E., Polishuk, I., Canales, R.I., Quinteros-Lama, H., Garrido, J.M., 2022. Interfacial properties of fluorinated (f)-gases in azeotropic condition. J. Mol. Liq. 350, 118604. http://dx.doi.org/10.1016/j.molliq.2022.118604.

Gubbins, K.E., Twu, C.H., 1978. Thermodynamics of polyatomic fluid mixtures—I theory. Chem. Eng. Sci. 33 (7), 863–878. http://dx.doi.org/10.1016/0009-2509(78)85176-8.

Hockney, R.W., Eastwood, J.W., 1988. Computer Simulation using Particles, first ed. CRC Press, http://dx.doi.org/10.1201/9780367806934.

Hulse, R.J., Basu, R.S., Singh, R.R., Thomas, R.H., 2012. Physical properties of HCFO-1233zd(E). J. Chem. Eng. Data 57 (12), 3581–3586. http://dx.doi.org/10.1021/je300776s.

IPCC, 2022. Climate Change 2022: Impacts, Adaptation, and Vulnerability. Contribution of Working Group II to the Sixth Assessment Report of the Intergovernmental Panel on Climate Change. Tech. rep., Cambridge University Press.

Irving, J.H., Kirkwood, J.G., 1950. The statistical mechanical theory of transport processes, IV. The equations of hydrodynamics. J. Chem. Phys. 18 (6), 817–829. http://dx.doi.org/10.1063/1.1747782.

Janeček, J., 2006. Long range corrections in inhomogeneous simulations. J. Phys. Chem. B 110 (12), 6264–6269. http://dx.doi.org/10.1021/jp056344z.

Johnson, J., Müller, E.A., Gubbins, K.E., 1994. Equation of state for Lennard-Jones chains. J. Phys. Chem. 98 (25), 6413–6419. http://dx.doi.org/10.1021/j100076a028.

Johnson, J., Zollweg, J., Gubbins, K.E., 1993. The Lennard-Jones equation of state revisited. Mol. Phys. 78 (3), 591–618. http://dx.doi.org/10.1080/00268979300100411.

Jovell, D., Gómez, S.B., Zakrzewska, M.E., Nunes, A., Araújo, J., Pereiro, A.B., Llovell, F., 2020. Insight on the solubility of R134a in fluorinated ionic liquids and deep eutectic solvents. J. Chem. Eng. Data 65 (10), 4956–4969. http://dx.doi.org/10.1021/acs.jced.0c00588.

Kano, Y., Kayukawa, Y., Fujii, K., Sato, H., 2010. Ideal-gas heat capacity for 2 3, 3 3-Tetrafluoropropene (HFO-1234yf) Determined from speed-of-sound measurements. Int. J. Thermophys. 31 (11–12), 2051–2058. http://dx.doi.org/10.1007/s10765-010-0885-7.

Kelkar, M.S., Shiflett, M.B., Yokozeki, A., Maginn, E.J., 2008. Development of force fields for hydrofluorocarbons. In: AIChE Annu, Meeting. Philadelphia, USA, pp. 1–200.

Klein, S., McLinden, M., Laesecke, A., 1997. An improved extended corresponding states method for estimation of viscosity of pure refrigerants and mixtures. Int. J. Refrig. 20 (3), 208–217. http://dx.doi.org/10.1016/S0140-7007(96)00073-4.

Lemmon, E.W., Bell, I.H., Huber, M.L., McLinden, M.O., 2018. NIST Standard Reference Database 23: Reference Fluid Thermodynamic and Transport Properties-REFPROP, Version 10.0. National Institute of Standards and Technology, http://dx.doi.org/10.18434/T4/1502528, URL https://www.nist.gov/srd/refprop.

Lennard-Jones, J.E., 1931. Cohesion. Proc. Phys. Soc. 43 (240), 461–482.

Li, Y., Fouad, W.A., Vega, L.F., 2019. Interfacial anomaly in low global warming potential refrigerant blends as predicted by molecular dynamics simulations. Phys. Chem. Chem. Phys. 21 (39), 22092–22102. http://dx.doi.org/10.1039/C9CP03231B.

Llovell, F., Marcos, R.M., Vega, L.F., 2013. Transport properties of mixtures by the soft-saft + free-volume theory: Application to mixtures of n-alkanes and hydrofluorocarbons. J. Phys. Chem. B 117 (17), 5195–5205. http://dx.doi.org/10.1021/jp401754r.

Llovell, F., Vega, L.F., 2007. Phase equilibria, critical behavior and derivative properties of selected n-alkane/n-alkane and n-alkane/1-alkanol mixtures by the crossover soft-saft equation of state. J. Supercrit. Fluids 41 (2), 204–216.

Martínez-Ruiz, F.J., Moreno-Ventas Bravo, A.I., Blas, F.J., 2015. Liquid-liquid interfacial properties of a symmetrical Lennard-Jones binary mixture. J. Chem. Phys. 143 (10), 104706. http://dx.doi.org/10.1063/1.4930276.

Martyna, G.J., Tobias, D.J., Klein, M.L., 1994. Constant pressure molecular dynamics algorithms. J. Chem. Phys. 101 (5), 4177–4189. http://dx.doi.org/10.1063/1.467468.

McLinden, M.O., Klein, S.A., Perkins, R.A., 2000. An extended corresponding states model for the thermal conductivity of refrigerants and refrigerant mixtures. Int. J. Refrig. 23 (1), 43–63.

Mejía, A., Segura, H., 2004. Interfacial behavior in type IV systems. Int. J. Thermophys. 25 (5), 1395–1414. http://dx.doi.org/10.1007/s10765-004-5746-9.

Mota-Babiloni, A., Makhnatch, P., Khodabandeh, R., 2017. Recent investigations in HFCs substitution with lower gwp synthetic alternatives: Focus on energetic performance and environmental impact. Int. J. Refrig. 82, 288–301. http://dx.doi.org/10.1016/j.ijrefrig.2017.06.026.

Müller, E.A., Ervik, A., Mejía, A., 2021. A guide to computing interfacial properties of fluids from molecular simulations [article v1.0]. Living J. Comput. Mol. Sci. 2 (1), 21385. http://dx.doi.org/10.33011/livecoms.2.1.21385.

Nosé, S., 1984. A molecular dynamics method for simulations in the canonical ensemble. Mol. Phys. 52 (2), 255–268. http://dx.doi.org/10.1080/00268978400101201.

Opteon™ Solutions, 2021. Opteon™ refrigerants. URL https://www.opteon.com/en/products/refrigerants.

Outcalt, S.L., McLinden, M.O., 1995. Equations of state for the thermodynamic properties of R32 (difluoromethane) and R125 (pentafluoroethane). Int. J. Thermophys. 16-16 (1), 79–89. http://dx.doi.org/10.1007/BF01438959.

Peguin, R.P.S., Kamath, G., Potoff, J.J., da Rocha, S.R.P., 2009. All-atom force field for the prediction of vapor-liquid equilibria and interfacial properties of HFA134a. J. Phys. Chem. B 113 (1), 178–187. http://dx.doi.org/10.1021/jp806213w.

Petr, P., Raabe, G., 2015. Evaluation of R-1234ze(Z) as drop-in replacement for R-245fa in Organic Rankine Cycles – From thermophysical properties to cycle performance. Energy 93, 266–274. http://dx.doi.org/10.1016/j.energy.2015.09.035.

Polishuk, I., 2012. Modeling of viscosities in extended pressure range using SAFT + Cubic EoS and modified Yarranton-Satyro correlation. Ind. Eng. Chem. Res. 51 (41), 13527–13537. http://dx.doi.org/10.1021/ie3021208.

Potter, S.C., Tildesley, D.J., Burgess, A.N., Rogers, S.C., 1997. A transferable potential model for the liquid-vapour equilibria of fluoromethanes. Mol. Phys. 92 (5), 825–834. http://dx.doi.org/10.1080/002689797169772, URL https://www.tandfonline.com/doi/abs/10.1080/002689797169772.

Raabe, G., 2012. Molecular modeling of fluoropropene refrigerants. J. Phys. Chem. B 116 (19), 5744–5751. http://dx.doi.org/10.1021/jp300991t.

Raabe, G., 2013. Molecular simulation studies on the vapor–liquid phase equilibria of binary mixtures of R-1234yf and R-1234ze(E) with R-32 and CO2. J. Chem. Eng. Data 58 (6), 1867–1873. http://dx.doi.org/10.1021/je4002619.

Raabe, G., 2014. Molecular dynamics studies on liquid-phase dynamics and structures of four different fluoropropenes and their binary mixtures with R-32 and CO2. J. Phys. Chem. B 118 (1), 240–254. http://dx.doi.org/10.1021/jp409408k.

Raabe, G., 2015. Molecular Simulation Studies on the Vapor–Liquid Equilibria of the cis - and trans -HCFO-1233zd and the cis - and trans -HFO-1336mzz. J. Chem. Eng. Data 60 (8), 2412–2419. http://dx.doi.org/10.1021/acs.jced.5b00286.

Raabe, G., 2016. Molecular simulation studies in hydrofluoroolefine (HFO) working fluids and their blends. Sci. Technol. Built Environ. 22 (8), 1077–1089. http://dx.doi.org/10.1080/23744731.2016.1206796.

Raabe, G., 2017. Molecular Simulation Studies on Thermophysical Properties with Application to Working Fluids, first ed. Springer, Singapore, http://dx.doi.org/10.1007/978-981-10-3545-6.

Raabe, G., 2019. Molecular simulation studies on refrigerants past – present – future. Fluid Phase Equilib. 485, 190–198. http://dx.doi.org/10.1016/j.fluid.2018.12.022.

Raabe, G., 2020. Parameterization approach for a systematic extension of the hydrofluoroolefin force field to fluorinated butenes and hydrochlorofluoroolefin compounds. J. Chem. Eng. Data 65 (3), 1234–1242. http://dx.doi.org/10.1021/acs.jced.9b00588.

Raabe, G., Maginn, E.J., 2010a. A force field for 3 3, 3-fluoro-1-propenes, including HFO-1234yf. J. Phys. Chem. B 114 (31), 10133–10142. http://dx.doi.org/10.1021/jp102534z.

Raabe, G., Maginn, E.J., 2010b. Molecular modeling of the vapor–liquid equilibrium properties of the alternative refrigerant 2 3, 3 3-tetrafluoro-1-propene (hfo-1234yf). J. Phys. Chem. Lett. 1 (1), 93–96. http://dx.doi.org/10.1021/jz900070h.

2024. Regulation (EU) 2024/573 of the European parliament and of the council of 7 2024 on fluorinated greenhouse gases, amending directive (EU) 2019/1937 and repealing regulation (EU) no 517/2014 (text with EEA relevance). Of. J. Eur. Union.

Schneider, T., Stoll, E., 1978. Molecular-dynamics study of a three-dimensional one-component model for distortive phase transitions. Phys. Rev. B 17 (3), 1302–1322. http://dx.doi.org/10.1103/PhysRevB.17.1302.

Sheng, B., Zhao, Y., Dong, X., Yan, H., Zhong, Q., Wang, J., Shen, J., Gong, M., 2021. A corresponding state equation for compressed liquid isochoric heat capacity of pure and mixture refrigerants. Int. J. Refrig. 124, 20–29. http://dx.doi.org/10.1016/j.ijrefrig.2020.12.016.

Stell, G., Rasaiah, J.C., Narang, H., 1972. Thermodynamic perturbation theory for simple polar fluids - I. Mol. Phys. 23 (2), 393–406. http://dx.doi.org/10.1080/00268977200100381.

Thompson, A.P., Aktulga, H.M., Berger, R., Bolintineanu, D.S., Brown, W.M., Crozier, P.S., in 't Veld, P.J., Kohlmeyer, A., Moore, S.G., Nguyen, T.D., Shan, R., Stevens, M.J., Tranchida, J., Trott, C., Plimpton, S.J., 2022. LAMMPS - a flexible simulation tool for particle-based materials modeling at the atomic, meso, and continuum scales. Comput. Phys. Comm. 271, 108171. http://dx.doi.org/10.1016/j.cpc.2021.108171.

Twu, C., Gubbins, K.E., 1978. Thermodynamics of polyatomic fluid mixtures—II: Polar, quadrupolar and octopolar molecules. Chem. Eng. Sci. 33 (7), 879–887. http://dx.doi.org/10.1016/0009-2509(78)85177-X.

United Nations Environment Programme Ozone Secretariat, 2020. Handbook for the Montreal Protocol on Substances that Deplete the Ozone Layer, fourteenth ed. UN Environment Programme, Nairobi, Kenya, xURL https://ozone.unep.org/treaties/montreal-protocol.

United States Environmental Protection Agency, 2020. Inventory of Greenhouse Gas Emissions and Sinks 1990-2018. EPA Report.

Vilaseca, O., Llovell, F., Yustos, J., Marcos, R., Vega, L., 2010. Phase equilibria, surface tensions and heat capacities of hydrofluorocarbons and their mixtures including the critical region. J. Supercrit. Fluids 55 (2), 755–768. http://dx.doi.org/10.1016/j.supflu.2010.10.015, 100th year Anniversary of van der Waals' Nobel Lecture.

Waals, J., 1891. Théorie Moléculaire D'une Substance Composée de Deux Matières Différentes. In: Archives Néerlandaises des Sciences Exactes et Naturelles, Vol. 24, Société Hollandaise des Sciences: The Hague, Archives Néerlandaises des Sciences. Exactes et Naturelles Société Hollandaise des Sciences, The Hague.

van der Waals, J.D., 1894. Thermodynamische theorie der kapillarität unter voraussetzung stetiger dichteänderung. Z. Phys. Chem. 13U (1), 657–725. http://dx.doi.org/10.1515/zpch-1894-1338.

Wang, N., Carlozo, M.N., Marin-Rimoldi, E., Befort, B.J., Dowling, A.W., Maginn, E.J., 2023. Machine learning-enabled development of accurate force fields for refrigerants. J. Chem. Theory Comput. 19 (14), 4546–4558. http://dx.doi.org/10.1021/acs.jctc.3c00338.

Xiao, X., Kim, D., Jiao, F., Yang, X., Al Ghafri, S., Siahvashi, A., Tsuji, T., Yukumoto, A., Seiki, Y., Stanwix, P.L., May, E.F., 2023. Viscosity, thermal conductivity, and interfacial tension study of CO_2 + difluoromethane (r32). Int. J. Refrig. 152, 331–342. http://dx.doi.org/10.1016/j.ijrefrig.2023.04.019.

Zeiger, B., Gschrey, B., Kauffeld, M., 2016. Riefing Paper: Availability of Alternatives to HFCs in Commercial Refrigeration in the EU. Öko-Recherche.

Zhang, Y., Otani, A., Maginn, E.J., 2015. Reliable viscosity calculation from equilibrium molecular dynamics simulations: A time decomposition method. J. Chem. Theory Comput. 11 (8), 3537–3546. http://dx.doi.org/10.1021/acs.jctc.5b00351.

Zhelezny, V., Sechenyh, V., Ivchenko, D., Semenyuk, Y., 2014. Prediction of the surface tension for refrigerants and refrigerant-oil solutions (ROS). Int. J. Refrig. 40, 241–245. http://dx.doi.org/10.1016/j.ijrefrig.2013.12.003.